scattering factors were used, with anomalous dispersion corrections applied.[18] No corrections for extinction were made. The data were corrected for absorption by using an empirical ψ scan method ($T_{max} = 1$; $T_{min} = 0.208$). All non-hydrogen atoms were refined anisotropically; hydrogen atoms were not included in the model. The model converged at $R = 0.061$. The final values of the refined positional parameters are presented in Table II. All other supporting data are available as supplementary material. The final full-matrix least-squares refinement cycles used a weighting scheme of $w = 1/(\sigma^2(F) + 0.0031F^2)$. All calculations were carried out at Montana State University (by J.F.F.) using the program package XTAL2.6,[19] on a micro Vax cluster.

$[PPh_4][Cl_3W(\mu\text{-}THT)_2(\mu\text{-}S(CH_2)_4Cl)WCl_3]$. Well-formed, needle-shaped crystals were grown from a saturated acetone solution of **4** by slow evaporation of the solvent. A portion of one of these needles was cut and mounted on a glass fiber. Accurate cell dimensions and a crystal orientation matrix were determined on an Enraf-Nonius CAD4 diffractometer, by a least-squares refinement of the setting angles of 25 reflections in the θ range, 10–15°. Data were collected in the ω–2θ scan mode. Three reflections were monitored every 2 h of exposure time, and a linear loss of intensity (1.8%) was corrected for by appropriate scaling. Data were corrected for absorption effects (DIFABS[20]); correction factors were in the range 0.688–1.237. All other pertinent data are given in Tables IV and SIII. The structure was solved by direct methods. It was refined by full-matrix least-squares calculations, initially with isotropic and finally with anisotropic temperature factors for the non-hydrogen atoms, except for the chlorobutyl group. This was disordered over two sites with site occupancy factors of 0.4 and 0.6. The C(1)–C(4) and Cl(7) atoms were allowed to refine with isotropic temperature factors. Refinement converged with $R = 0.040$ and $R_w = 0.045$. Scattering factors were taken from Cromer and Mann,[21] and allowance was made for anomalous dispersion.[22] A difference map calculated at the end of the refinement showed maxima at positions expected for hydrogen atoms, but these were not included in the model. There were no other chemically significant features. All the crystallographic calculations (by M.P.) were carried out by using XTAL2.6;[19] Figure 2 was plotted by using ORTEP II.[23]

Acknowledgment. We thank the Natural Sciences and Engineering Research Council of Canada for the award of an operating grant (to P.M.B.) and an infrastructure grant.

Supplementary Material Available: Tables SI–SVI, listing complete crystallographic data, thermal parameters, and additional bond lengths and angles for **3** and **4** (13 pages); tables of observed and calculated structure factors (81 pages). Ordering information is given on any current masthead page.

---

(18) *International Tables of Crystallography*; Kynoch Press: Birmingham, U.K., 1974; Vol. 4.
(19) *XTAL2.6 User's Manual*; Hall, S. R.; Stewart, J. M., Eds.; Universities of Western Australia and Maryland, 1989.
(20) Walker, N.; Stewart, D. DIFABS. *Acta Crystallogr.* **1983**, *A39*, 158.
(21) Cromer, D. T.; Mann, J. B. *Acta Crystallogr.* **1968**, *A24*, 321.
(22) Cromer, D. T.; Liberman, D. *J. Chem. Phys.* **1970**, *53*, 1891.
(23) Johnson, C. K. ORTEP II. Report ORNL-5138; Oak Ridge National Laboratory: Oak Ridge, TN, 1976.

Contribution from the Departments of Chemistry, National Tsing Hua University,
Hsinchu, Taiwan, ROC, and National Taiwan University, Taipei, Taiwan, ROC

Stereochemical Nonrigidity in Six-Coordinate Monochelate Complexes via Polytopal Rearrangement

C. Y. Lee,*,† Y. Wang,‡ and C. S. Liu*,†

Received August 15, 1990

Analysis of the ^{19}F, ^{13}C, and ^{31}P NMR data for $F_2\overline{SiC(t\text{-}Bu){=}CHSiF_2Fe}(CO)_3(phosphine)$ (phosphine = PMe_3, PPh_2Me, PPh_3, and PEt_3, for compounds **3**–**6**, respectively) over a temperature range covering slow and fast exchange characterizes those complexes as stereochemically nonrigid on the NMR time scale. The activation parameters for the rearrangement process are $\Delta G^* = 16.8$, 15.0, 12.5, and 13.2 kcal/mol for complexes **3**–**6**, respectively. The crystal and molecular structures of **3b** and **5a** were determined. The molecular structures are best described as distorted octahedra. The space group of both **3b** and **5a** is $Pca2_1$: $a = 15.617$ (3) Å, $b = 8.161$ (3) Å, $c = 29.858$ (4) Å, and $Z = 8$ for **3b**; $a = 17.409$ (8) Å, $b = 9.439$ (2) Å, $c = 17.332$ (5) Å, and $Z = 4$ for **5a**. The intramolecular ligand permutations are interpreted in terms of the "trigonal-twist" mechanism.

It is generally accepted that six-coordinate complexes in solution may undergo permutation of ligand positions via either a bond-breaking process or an intramolecular polytopal rearrangement.[1,2] The established cases of polytopal rearrangement of octahedral complexes are rare in the literature and sometimes inconclusive. Most of these cases involve tris-chelate and bis-chelate derivatives where the trigonal-twist mechanism was considered to be the most likely mechanism for the isomerization.[3-8]

The nonchelate metal complexes $M(CO)_4(ER_3)_2$ (M = Fe, Ru, Os; E = Si, Ge, Sn, Pb) have been known for their fluxional behavior in solutions.[9] The study of the ^{13}C NMR spectral pattern of coalescence in cis–trans mixtures strongly suggests that axial–equatorial averaging proceeds via a cis-to-trans-to-cis isomerization process. This mechanism is further supported by the observation that monochelate complexes $Me_2\overline{SiCH_2CH_2SiMe_2Fe}(CO)_4$ do not show fluxional behavior in solutions, since the chelate ring would not allow a trans configuration.[10]

On the other hand, if a six-coordinate complex adopts the geometry of a highly distorted octahedron, other pathways of intramolecular rearrangement are possible. For example in the case of highly twisted octahedral complex $H_2Fe(PPh_3)_4$, the permutation mechanism was proposed to be a "tetrahedral jump".[11]

In the case of monochelate octahedral complexes, the stereochemical nonrigidity has been much less understood. One fluxional

---

† National Tsing Hua University.
‡ National Taiwan University.

(1) Muetterties, E. L. *J. Am. Chem. Soc.* **1969**, *91*, 1636.
(2) Muetterties, E. L. *Acc. Chem. Res.* **1970**, *3*, 266.
(3) Pignolet, L. H.; Lewis, R. A.; Holm, R. H. *J. Am. Chem. Soc.* **1971**, *93*, 360.
(4) Eeaton, S. S.; Eaton, G. R.; Holm, R. H.; Muetterties, E. L. *J. Am. Chem. Soc.* **1973**, *95*, 1116.
(5) Muetterties, E. L. *J. Am. Chem. Soc.* **1968**, *90*, 5097.
(6) Hathaway, B.; Duggan, M.; Murphy, A.; Mullane, J.; Power, C.; Walsh, A.; Walsh, B. *Coord. Chem. Rev.* **1981**, *36*, 267.
(7) Fay, R. C.; Lindmark, A. F. *J. Am. Chem. Soc.* **1983**, *105*, 2118.
(8) Ismail, A. A.; Sauriol, F.; Sedman, J.; Butler, I. S. *Organometallics* **1985**, *4*, 1914.
(9) Vancea, L.; Pomery, R. K.; Graham, W. A. G. *J. Am. Chem. Soc.* **1976**, *98*, 1407.
(10) Vancea, L.; Graham, W. A. G. *Inorg. Chem.* **1974**, *13*, 511.
(11) Meakin, P.; Muetterties, E. L.; Jesson, J. P. *J. Am. Chem. Soc.* **1973**, *95*, 75.
(12) Vacea, L.; Bennet, M. J.; Jones, C. E.; Smith, R. A.; Graham, W. A. G. *Inorg. Chem.* **1977**, *16*, 897.

system that has been well studied is that of the derivatives of methyltitanium trichloride $\overline{XCH_2CH_2YTi}(CH_3)Cl_3$, with X and Y being OCH_3, $N(CH_3)_2$, SCH_3, etc. It was found that they undergo isomerization in solution.[13]

The variable-temperature NMR studies suggested that the interconversion of the two meridional isomers (Ia and Ib) could be achieved by the process of a trigonal twist, a result that was considered inconclusive because only one meridional form was observed in the low-temperature-limiting spectrum.[14]

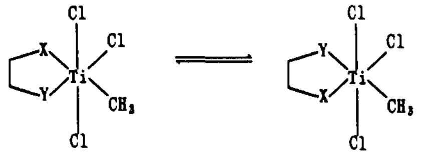

Ia Ib

In an attempt to understand the permutation pathway of monochelate six-coordinate complexes, a series of monochelate complexes $\overline{F_2SiC(t\text{-Bu})=CHSiF_2Fe}(CO)_3$(phosphine) were prepared and studied by X-ray diffraction and NMR at various temperatures.

If one takes advantage of there being four different kinds of nuclei that are routinely NMR operative (^1H, ^{19}F, ^{13}C, ^{31}P), the fluxional behavior of these complexes can be studied in detail. It was hoped that the systematic study of these fluxional phenomena would give more conclusive insight about the mechanism of the ligand permutations of monochelate six-coordinate complexes.

Results

Monochelate complexes $\overline{F_2SiC(t\text{-Bu})=CHSiF_2Fe}(Co)_3$(phosphine) are prepared by the following reactions:

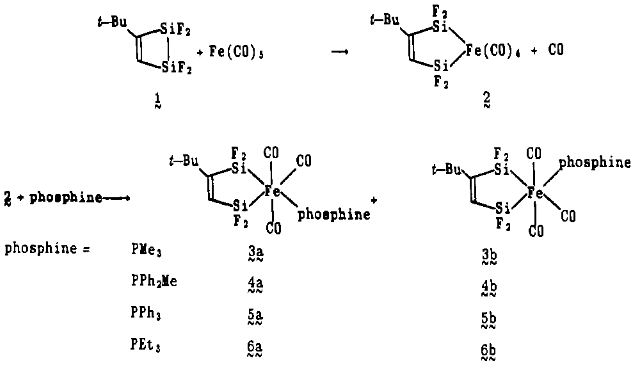

Complexes **3a**/**3b**, **4a**/**4b**, **5a**/**5b**, and **6a**/**6b** are identified by elemental analyses, mass spectra, and ^1H, ^{19}F, ^{13}C, and ^{31}P NMR spectra. The low-temperature-limiting spectra show that each sample contains a pair of isomers of the octahedral complex, with both "axial" positions occupied by carbonyl groups (vide infra). The structure determination is made possible by the fact that only trans SiF_2/phosphine and trans SiF_2/CO would cause significant ^{19}F–^{31}P and ^{19}F–^{13}C couplings. Cis arrangements of these ligands would show either very small or nonobservable couplings.

(A) Crystal Structures of 3b and 5a. Since both compounds **3b** and **5a** were obtained as single crystals, X-ray diffraction experiments were carried out. A view of the molecules with atom numbering schemes is depicted in Figure 1. Crystallographic data are given in Tables I–III. Selected bond distances and angles are given in Tables IV and V for **3b** and **5a**, respectively. The overall features of these two compounds are very similar, differing only in the relative position of the phosphine ligand. In each case, the metal is six-coordinate, adopting a distorted octahedral geometry. Two CO groups occupy the axial positions, while the two silicon atoms, the phosphorus atom, and the other CO constitute the equatorial plane. The angles between the axial carbonyl carbons (C(8)–Fe–C(9)) for **3b** and **5a** are 168 (1) and 163.6 (11)°, respectively. Compared with the corresponding angles in *cis*-$Fe(CO)_4(SiMe_3)_2$ (141.2°)[12] and *cis*-$Fe(CO)_4(SnPh_3)_2$ (159.6°),[15] which have been described as "pseudo-bicapped

Table I. Crystal Data

compd	**3b**	**5a**
formula	$C_{12}H_{19}Si_2F_4O_3PFe$	$C_{27}H_{25}Si_2F_4O_3PFe$
fw	430.3	616.5
space group	*Pca*2$_1$	*Pca*2$_1$
a, Å	15.617 (3)	17.490 (8)
b, Å	8.161 (3)	9.439 (2)
c, Å	29.858 (4)	17.332 (5)
V, Å^3	3805 (2)	2862 (2)
Z	8	4
λ, Å	0.7107	0.7107
μ, mm^{-1}	1.04	0.71
transm coeff	0.85–1.0	0.96–1.0
D_{cal}, g·cm^{-3}	1.520	1.431
R(*F*)	0.071	0.061
$R_w(F)$	0.065	0.067
cryst size, mm	0.13 × 0.20 × 0.65	0.13 × 0.40 × 0.50
$2\theta_{max}$, deg	50	50
2θ scan params	2(0.65 + 0.35 tan θ)	2(0.65 + 0.35 tan θ)
tot. no. of measmts	3415	2615
no. of obsd reflns (>3σ)	1876	1217

Table II. Atomic Parameters *x*, *y*, *z* and B_{iso} Values for **3b**, Where Esd's Refer to the Last Digit Printed

	x	*y*	*z*	B_{iso}, Å^2
Fe(1A)	0.02750 (18)	0.2002 (4)	0.54044	2.85 (13)
P(1A)	−0.0609 (4)	−0.0085 (8)	0.56104 (19)	3.4 (3)
Si(1A)	0.0753 (5)	0.2405 (9)	0.61224 (19)	3.9 (3)
Si(2A)	0.1189 (4)	0.4069 (8)	0.52683 (20)	3.5 (3)
F(11A)	−0.0018 (9)	0.2571 (21)	0.6472 (4)	8.4 (10)
F(12A)	0.1284 (12)	0.0877 (16)	0.6323 (5)	8.8 (10)
F(21A)	0.1978 (8)	0.3551 (16)	0.4930 (4)	5.0 (7)
F(22A)	0.0767 (9)	0.5664 (16)	0.5046 (4)	6.5 (8)
C(1A)	0.1499 (14)	0.420 (3)	0.6180 (6)	3.4 (5)
C(2A)	0.1665 (15)	0.481 (3)	0.5803 (7)	4.4 (5)
C(3A)	0.1829 (15)	0.479 (3)	0.6639 (7)	4.7 (6)
C(4A)	0.220 (3)	0.595 (5)	0.6607 (13)	16.2 (16)
C(5A)	0.0898 (19)	0.524 (4)	0.6950 (8)	6.8 (7)
C(6A)	0.250 (3)	0.387 (5)	0.6738 (13)	16.2 (16)
C(7A)	0.0001 (14)	0.197 (3)	0.4841 (6)	4.1 (5)
C(8A)	−0.0475 (14)	0.348 (3)	0.5564 (7)	4.3 (6)
C(9A)	0.1127 (13)	0.068 (3)	0.5340 (7)	4.0 (5)
C(10A)	−0.1074 (16)	−0.126 (3)	0.5155 (7)	5.4 (6)
C(11A)	−0.1535 (15)	0.035 (3)	0.5912 (7)	4.4 (5)
C(12A)	−0.0134 (17)	−0.177 (4)	0.5889 (8)	7.0 (8)
O(1A)	−0.0159 (9)	0.2025 (20)	0.4458 (4)	4.4 (3)
O(2A)	−0.0994 (10)	0.4489 (21)	0.5634 (5)	5.8 (4)
O(3A)	0.1689 (9)	−0.0214 (19)	0.5318 (4)	4.7 (4)
Fe(1B)	0.24037 (19)	0.6972 (4)	0.39070 (10)	2.80 (12)
P(1B)	0.3249 (4)	0.4878 (8)	0.37113 (19)	3.6 (3)
Si(1B)	0.1909 (4)	0.7402 (9)	0.31896 (20)	4.2 (3)
Si(2B)	0.1490 (5)	0.9129 (9)	0.40465 (19)	4.3 (3)
F(11B)	0.2649 (10)	0.7471 (22)	0.2851 (4)	8.2 (10)
F(12B)	0.1385 (11)	0.5865 (19)	0.2986 (4)	8.3 (10)
F(21B)	0.0748 (9)	0.8745 (17)	0.4374 (4)	5.9 (8)
F(22B)	0.1912 (9)	1.0570 (15)	0.4301 (3)	5.3 (7)
C(1B)	0.1207 (13)	0.927 (3)	0.3140 (6)	3.3 (5)
C(2B)	0.0961 (13)	0.993 (3)	0.3551 (6)	2.9 (4)
C(3B)	0.0828 (14)	0.989 (3)	0.2700 (7)	4.1 (5)
C(4B)	0.0634 (20)	1.165 (4)	0.2667 (9)	8.6 (9)
C(5B)	0.0227 (24)	0.856 (5)	0.2569 (11)	13.0 (13)
C(6B)	0.1210 (20)	0.931 (4)	0.2312 (9)	8.7 (9)
C(7B)	0.2649 (13)	0.694 (3)	0.4489 (6)	3.4 (4)
C(8B)	0.3190 (14)	0.850 (3)	0.3777 (7)	4.4 (6)
C(9B)	0.1490 (14)	0.559 (3)	0.3959 (7)	4.1 (5)
C(10B)	0.3638 (16)	0.380 (3)	0.4176 (7)	5.1 (6)
C(11B)	0.4161 (15)	0.546 (3)	0.3347 (7)	4.8 (6)
C(12B)	0.2755 (15)	0.322 (3)	0.3356 (7)	5.1 (6)
O(1B)	0.2858 (10)	0.7033 (22)	0.4859 (5)	5.5 (4)
O(2B)	0.3657 (12)	0.9465 (22)	0.3658 (5)	7.3 (5)
O(3B)	0.0977 (11)	0.4684 (22)	0.3957 (5)	7.1 (5)

---

(13) Clark, R. J. H.; McAlees, A. J. *Inorg. Chem.* **1972**, *11*, 342.

(14) Holm, R. H. In *Dynamic Nuclear Magnetic Resonance Spectroscopy*; Jackman, L. M., Cotton, F. A., Eds.; Academic Press: New York, 1975; Chapter 9, pp 331–332.

Table III. Atomic Parameters x, y, z and B_{iso} Values for **5a**, Where Esd's Refer to the Last Digit Printed

	x	y	z	B_{iso}, Å^2
Fe	0.20575 (14)	0.10211 (25)	0.25000	4.19 (12)
P	0.1723 (3)	0.2698 (5)	0.1636 (3)	3.38 (21)
Si(1)	0.2307 (3)	−0.0513 (6)	0.3510 (4)	5.3 (3)
Si(2)	0.3211 (3)	0.0228 (7)	0.2101 (4)	6.1 (3)
F(11)	0.1628 (6)	−0.1568 (12)	0.3652 (9)	9.0 (8)
F(12)	0.2365 (8)	0.0283 (13)	0.4315 (7)	9.5 (8)
F(21)	0.3166 (7)	−0.0414 (13)	0.1241 (6)	9.1 (8)
F(22)	0.3871 (6)	0.1367 (12)	0.2050 (7)	8.1 (7)
C(1)	0.3202 (10)	−0.1551 (17)	0.3404 (13)	5.7 (11)
C(2)	0.3555 (12)	−0.1176 (20)	0.2709 (13)	7.4 (13)
C(3)	0.3487 (11)	−0.2645 (19)	0.3982 (12)	6.1 (12)
C(4)	0.4013 (14)	−0.3676 (25)	0.3595 (20)	11.9 (20)
C(5)	0.393 (3)	−0.194 (3)	0.4573 (16)	20.6 (31)
C(6)	0.2831 (13)	−0.361 (3)	0.4195 (18)	12.2 (19)
C(7)	0.1235 (12)	0.1222 (22)	0.3044 (12)	7.2 (6)
C(8)	0.1761 (13)	−0.0440 (24)	0.2002 (13)	8.6 (7)
C(9)	0.2591 (14)	0.2215 (21)	0.3002 (12)	7.2 (6)
C(1A)	0.2513 (10)	0.3574 (17)	0.1156 (10)	4.1 (9)
C(2A)	0.2960 (10)	0.2859 (18)	0.0640 (10)	4.6 (9)
C(3A)	0.3567 (11)	0.3497 (24)	0.0252 (10)	6.3 (12)
C(4A)	0.3774 (11)	0.490 (3)	0.0460 (12)	6.9 (12)
C(5A)	0.3327 (11)	0.5592 (20)	0.0999 (12)	5.9 (11)
C(6A)	0.2723 (10)	0.4982 (19)	0.1335 (10)	4.7 (9)
C(1B)	0.1166 (9)	0.4133 (16)	0.2038 (9)	3.7 (8)
C(2B)	0.1228 (10)	0.4531 (17)	0.2794 (10)	4.8 (10)
C(3B)	0.0812 (11)	0.5657 (19)	0.3089 (11)	5.6 (11)
C(4B)	0.0316 (10)	0.6414 (19)	0.2631 (12)	5.7 (11)
C(5B)	0.0263 (11)	0.6048 (20)	0.1889 (12)	6.9 (12)
C(6B)	0.0647 (11)	0.4932 (23)	0.1574 (11)	6.5 (12)
C(1C)	0.1100 (9)	0.2098 (16)	0.0848 (9)	3.1 (8)
C(2C)	0.1175 (9)	0.2529 (17)	0.0116 (10)	3.8 (9)
C(3C)	0.0643 (10)	0.2183 (22)	−0.0406 (10)	5.9 (11)
C(4C)	−0.0004 (11)	0.1417 (21)	−0.0215 (12)	6.3 (11)
C(5C)	−0.0104 (10)	0.0992 (21)	0.0517 (11)	5.9 (11)
C(6C)	0.0458 (9)	0.1310 (20)	0.1056 (9)	4.6 (10)
O(1)	0.0625 (9)	0.1254 (16)	0.3393 (10)	9.4 (4)
O(2)	0.1587 (8)	−0.1395 (15)	0.1622 (9)	8.8 (4)
O(3)	0.3010 (8)	0.2984 (16)	0.3340 (9)	8.6 (4)

Table IV. Selected Bond Distances (Å) and Angles (deg) for Compound **3b**

Fe(1A)–P(1A)	2.278 (7)	Fe(1B)–P(1B)	2.237 (7)
Fe(1A)–Si(1A)	2.294 (6)	Fe(1B)–Si(1B)	2.304 (7)
Fe(1A)–Si(2A)	2.247 (7)	Fe(1B)–Si(2B)	2.304 (7)
Fe(1A)–C(7A)	1.735 (20)	Fe(1B)–C(7B)	1.779 (18)
Fe(1A)–C(8A)	1.748 (22)	Fe(1B)–C(8B)	1.795 (23)
Fe(1A)–C(9A)	1.723 (22)	Fe(1B)–C(9B)	1.827 (22)
P(1A)–C(10A)	1.813 (24)	P(1B)–C(10B)	1.750 (24)
P(1A)–C(11A)	1.741 (23)	P(1B)–C(11B)	1.853 (24)
P(1A)–C(12A)	1.77 (3)	P(1B)–C(12B)	1.885 (24)
Si(1A)–F(11A)	1.599 (15)	Si(1B)–F(11B)	1.537 (15)
Si(1A)–F(12A)	1.612 (16)	Si(1B)–F(12B)	1.616 (17)
Si(1A)–C(1A)	1.882 (22)	Si(1B)–C(1B)	1.885 (22)
Si(2A)–F(21A)	1.648 (13)	Si(2B)–F(21B)	1.549 (14)
Si(2A)–F(22A)	1.602 (14)	Si(2B)–F(22B)	1.549 (14)
Si(2A)–C(2A)	1.863 (21)	Si(2B)–C(2B)	1.818 (20)
C(1A)–C(2A)	1.26 (3)	C(1B)–C(2B)	1.39 (3)
C(1A)–C(3A)	1.54 (3)	C(1B)–C(3B)	1.53 (3)
C(3A)–C(4A)	1.12 (5)	C(3B)–C(4B)	1.48 (4)
C(3A)–C(5A)	1.76 (4)	C(3B)–C(5B)	1.49 (5)
C(3A)–C(6A)	1.32 (5)	C(3B)–C(6B)	1.38 (3)
C(7A)–O(1A)	1.173 (23)	C(7B)–O(1B)	1.155 (23)
C(8A)–O(2A)	1.17 (3)	C(8B)–O(2B)	1.13 (3)
C(9A)–O(3A)	1.14 (3)	C(9B)–O(3B)	1.09 (3)

P(1A)–Fe(1A)–Si(1A)	92.99 (22)	P(1B)–Fe(1B)–Si(1B)	94.11 (24)
P(1A)–Fe(1A)–Si(2A)	174.62 (21)	P(1B)–Fe(1B)–Si(2B)	175.1 (3)
P(1A)–Fe(1A)–C(7A)	95.8 (8)	P(1B)–Fe(1B)–C(7B)	96.7 (7)
P(1A)–Fe(1A)–C(8A)	92.1 (7)	P(1B)–Fe(1B)–C(8B)	94.1 (7)
P(1A)–Fe(1A)–C(9A)	91.7 (7)	P(1B)–Fe(1B)–C(9B)	90.6 (7)
Si(1A)–Fe(1A)–Si(2A)	81.64 (24)	Si(1B)–Fe(1B)–Si(2B)	81.01 (24)
Si(1A)–Fe(1A)–C(7A)	171.2 (8)	Si(1B)–Fe(1B)–C(7B)	169.2 (7)
Si(1A)–Fe(1A)–C(8A)	82.2 (7)	Si(1B)–Fe(1B)–C(8B)	85.6 (7)
Si(1A)–Fe(1A)–C(9A)	86.7 (7)	Si(1B)–Fe(1B)–C(9B)	84.9 (7)
Si(2A)–Fe(1A)–C(7A)	89.6 (8)	Si(2B)–Fe(1B)–C(7B)	88.2 (7)
Si(2A)–Fe(1A)–C(8A)	87.5 (7)	Si(2B)–Fe(1B)–C(8B)	86.0 (7)
Si(2A)–Fe(1A)–C(9A)	87.6 (7)	Si(2B)–Fe(1B)–C(9B)	88.4 (7)
C(7A)–Fe(1A)–C(8A)	96.4 (10)	C(7B)–Fe(1B)–C(8B)	94.3 (10)
C(7A)–Fe(1A)–C(9A)	94.2 (10)	C(7B)–Fe(1B)–C(9B)	94.4 (9)
C(8A)–Fe(1A)–C(9A)	168.4 (10)	C(8B)–Fe(1B)–C(9B)	169.6 (10)

Table V. Bond Distances (Å) and Angles (deg) for Compound **5a**

Fe–P	2.256 (5)	C(8)–O(2)	1.16 (3)
Fe–Si(1)	2.313 (6)	C(9)–O(3)	1.19 (3)
Fe–Si(2)	2.260 (6)	C(1A)–C(2A)	1.37 (3)
Fe–C(7)	1.730 (21)	C(1A)–C(6A)	1.414 (24)
Fe–C(8)	1.708 (22)	C(2A)–C(3A)	1.39 (3)
Fe–C(9)	1.702 (21)	C(3A)–C(4A)	1.42 (3)
P–C(1A)	1.811 (18)	C(4A)–C(5A)	1.38 (3)
P–C(1B)	1.809 (17)	C(5A)–C(6A)	1.337 (25)
P–C(1C)	1.838 (16)	C(1B)–C(2B)	1.366 (23)
Si(1)–F(11)	1.570 (12)	C(1B)–C(6B)	1.428 (25)
Si(1)–F(12)	1.588 (13)	C(2B)–C(3B)	1.386 (24)
Si(1)–C(1)	1.855 (18)	C(3B)–C(4B)	1.38 (3)
Si(2)–F(21)	1.611 (13)	C(4B)–C(5B)	1.34 (3)
Si(2)–F(22)	1.579 (12)	C(5B)–C(6B)	1.36 (3)
Si(2)–C(2)	1.798 (20)	C(1C)–C(2C)	1.337 (23)
C(1)–C(2)	1.40 (3)	C(1C)–C(6C)	1.394 (23)
C(1)–C(3)	1.52 (3)	C(2C)–C(3C)	1.338 (23)
C(3)–C(4)	1.50 (3)	C(3C)–C(4C)	1.38 (3)
C(3)–C(5)	1.44 (3)	C(4C)–C(5C)	1.34 (3)
C(3)–C(6)	1.51 (3)	C(5C)–C(6C)	1.388 (24)
C(7)–O(1)	1.23 (3)		

P–Fe–Si(1)	172.05 (21)	Si(1)–Fe–C(9)	85.6 (7)
P–Fe–Si(2)	105.09 (21)	Si(2)–Fe–C(7)	160.9 (7)
P–Fe–C(7)	94.0 (7)	Si(2)–Fe–C(8)	81.3 (8)
P–Fe–C(8)	98.8 (8)	Si(2)–Fe–C(9)	83.5 (8)
P–Fe–C(9)	91.0 (7)	C(7)–Fe–C(8)	96.4 (10)
Si(1)–Fe–Si(2)	81.70 (23)	C(7)–Fe–C(9)	96.0 (10)
Si(1)–Fe–C(7)	79.2 (7)	C(8)–Fe–C(9)	163.6 (11)
Si(1)–Fe–C(8)	86.2 (8)		

tetrahedral" and "markedly distorted octahedral", respectively, the distortion in **3b** and **5a** is smaller. The average Fe–Si distance is 1.29 Å, which is comparable to those in $(F_2SiC(t\text{-}Bu)=CHSiF_2)Fe(C_6H_8)(CO)_2$ and $[(C_5H_5)FeSiF_2C(t\text{-}Bu)=CHSiF]_2$.[16,17] All three P–Fe–CO angles are larger than 90° (92, 93, 95°), consistent with the known fact that a CO group tends to tilt toward silyl groups.[18]

There are two molecules of **3b** in the asymmetric unit; the bond distances and angles of the two molecules are similar but with slight differences in the orientation of the *tert*-butyl and trimethylphosphine groups.

(B) Stereochemistry of 3a and 3b in Solution. The variable-temperature NMR spectra of these molecules show dynamic behavior. The spectra of isomers **3a**/**3b** are used to illustrate the results. A sample containing complexes **3a**/**3b** reached the low-limiting temperature at −50, −60, and −20 °C in its ^{13}C, ^{31}P, and ^{19}F NMR spectra, respectively. At −20 °C, the proton-noise-decoupled ^{19}F spectrum shows four resonances at 90.15 (F_b), 92.64 (F_a), 100.73 (F_a'), and 103.25 (F_b') ppm (shown in Figure 2). The five-membered ring is planar with the *tert*-butyl group in the plane, so the two fluorines in the same SiF_2 group are chemically equivalent. Since only trans $SiF_2/P(CH_3)_3$ would show significant P–F coupling, the doublets at 100.73 and 90.15 ppm are assigned

---

(15) Pomeroy, R. K.; Vancea, L.; Calhoun, H. P.; Graham, W. A. G. *Inorg. Chem.* **1977**, *16*, 1508.

(16) Hseu, T. H.; Lin, C. H.; Lee, C. Y.; Liu, C. S. *J. Chin. Chem. Soc.* **1989**, *36*, 91.

(17) Horng, K. M.; Wang, S. L.; Liu, C. S. *Organometallics* **1991**, *10*, 631.

(18) Berry, A. D.; Corey, E. R.; Hagen, A. P.; MacDiarmid, A. G.; Saalfeld, F. E.; Wayland, B. B. *J. Am. Chem. Soc.* **1970**, *92*, 1940.

(19) A broad peak at 200.83 ppm and a sharp peak at 200.05 ppm are observed in the ^{13}C NMR spectrum of **2**. When ^{19}F decoupling is applied, the peak at 200.83 ppm is resolved into two heavily overlapped peaks at 200.89 and 200.77 ppm. They are assigned to the equatorial carbonyls.

(20) Meakin, P.; Muetterties, E. L.; Tebbe, F. N.; Jesson, J. P. *J. Am. Chem. Soc.* **1971**, *93*, 4701.

(21) Liu, C. s.; Margrave, J. L.; Thompson, J. C. *Can. J. Chem.* **1972**, *50*, 465.

(22) Chi, Y.; Liu, C. S. *Inorg. Chem.* **1981**, *20*, 3456.

(23) Gabe, E. J.; LePage, Y.; White, P. S.; Lee, F. L. *Acta Crystallogr.* **1987**, *A43*, S294.

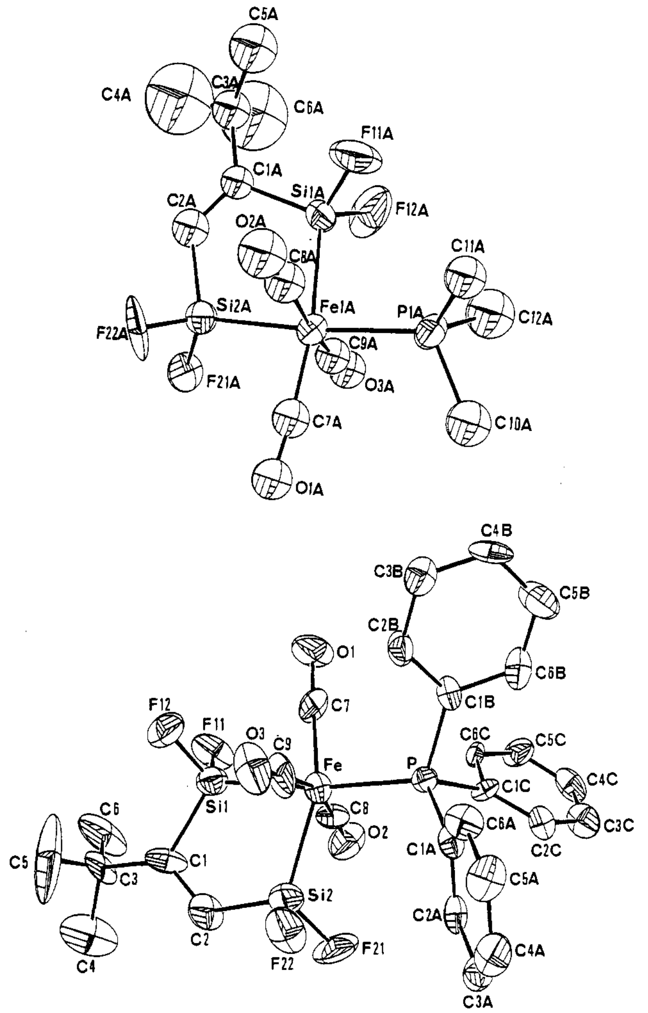

Figure 1. (a) Top: Molecular structure of compound **3b**. (Only one of the molecules in the asymmetric unit is shown.) (b) Bottom: Molecular structure of compound **5a**.

to the SiF_2 groups trans to $P(CH_3)_3$ in **3a** and **3b**, respectively. Compared with the nondecoupled ^{19}F spectrum, it is clear that the resonance at 90.15 ppm further couples with a proton and is assigned to $=CHSiF_2$ to **3b** whereas the resonance at 100.73 ppm is assigned to $=C(t\text{-}Bu)SiF_2$ of **3a** because no significant F–H coupling is observed. As temperature rises, all four peaks become broadened and finally merge into two peaks representing the average $F_a' \rightleftharpoons F_b'$ and $F_a \rightleftharpoons F_b$. Such exchanges among the SiF_2 groups of four different chemical environments are a typical consequence of isomerization between **3a** and **3b**. Equilibrium constants of **3a** ⇌ **3b** in a temperature range −80 to 0 °C can be estimated from the intensity ratio of the resonances in the spectra obtained at various temperatures. A plot of ln K_{eq} vs $1/T$ shows that ΔH equals 0.26 kcal/mol.[24]

The $^{31}P\{^1H\}$ spectrum of this system also shows dynamic behavior. At −60 °C, the spectrum of **3a**/**3b** shows two triplets for the two isomers (Figure 3a). The P–F couplings are due to the fluorines of the SiF_2 groups trans to the phosphine. When the temperature is raised, the spectrum broadens first and eventually sharpens to a triplet of triplets (resembling a quintet) due to P–F coupling with the two SiF_2 groups in the octahedral complex, which are averaged by rapid exchange (Figure 3b). The chemical shift in the high-temperature spectrum is the weighted average of these two isomers.

The temperature-dependent spectra of ^{13}C at the carbonyl region may serve as the main focal point in the interpretation of exchange mechanism. In principle there should be four signals for the CO groups of the two isomers. However, since the only difference between the two isomers is the position of the *tert*-butyl group relative to that of the phosphine, the chemical environments of the axial carbonyls of both isomers are nearly the same. In fact, even the equatorial carbonyls of the two isomers show very similar chemical shifts. For example, in the case of $\overline{F_2SiC(t\text{-}Bu)=CHSiF_2}Fe(CO)_4$ (**2**), where no fluxional behavior is observed in both ^{19}F and ^{13}C NMR spectra (−80 to +80 °C), only two signals (rather than three) with equal intensity are observed for the axial and two equatorial carbonyls (200.83 and 200.05 ppm). Obviously, the resonance signals for the two equatorial carbonyls are not resolved.[19]

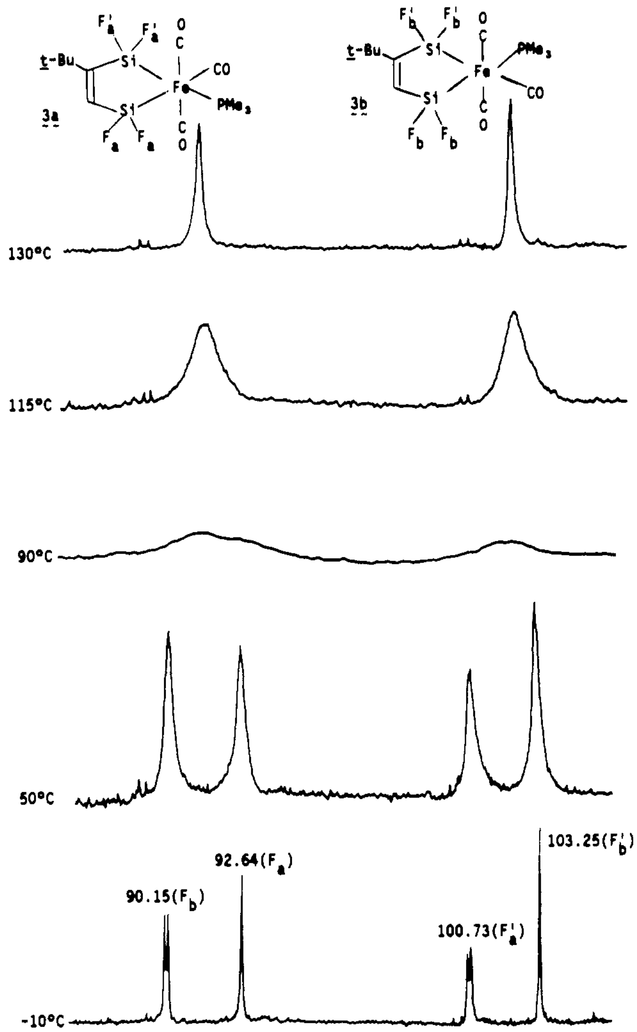

Figure 2. Temperature-dependent $^{19}F\{^1H\}$ NMR spectra of **3a** and **3b** (376.5 MHz). (A P–F coupling of 5.5 Hz is obtained from the high-temperature ^{31}P NMR spectrum (Figure 3), but it cannot be resolved in the ^{19}F NMR spectrum at 130 °C. However, the P–F coupling does show up in the high-temperature $^{19}F\{^1H\}$ NMR spectrum of **6a**/**6b**).

At −50 °C the ^{13}C spectrum of the carbonyl region shows two signals at 204.8 and 207.2 ppm, with an approximate intensity ratio 2:1, representing the four axial groups (204.8 ppm) and two equatorial CO groups (207.2 ppm) of two isomers **3a** and **3b** (Figure 4a). The assignments are made on the basis of the intensity ratio and the argument given above. It is clear that the signals for the CO_{eq} groups of **3a** and **3b** are not resolved. As the temperature is raised, the interconversion between isomers **3a** and **3b** becomes so rapid that carbonyl groups are indistinguishable in the NMR spectra. Hence, one observes the initial broadening of these two peaks and, as the fast-exchange limit is reached, the appearance of a new peak averaged at 205.6 ppm (Figure 4b). This exchange phenomenon is also shown in other spectral regions. For example, the high- and low-limiting ^{13}C spectra of PMe_3 are shown in Figure 4c,d.

---

[24] *a*/*b* ratio = 1.264 at 193 K, 1.27 at 213 K, 1.172 at 253 K, and 1.1 at 273 K.

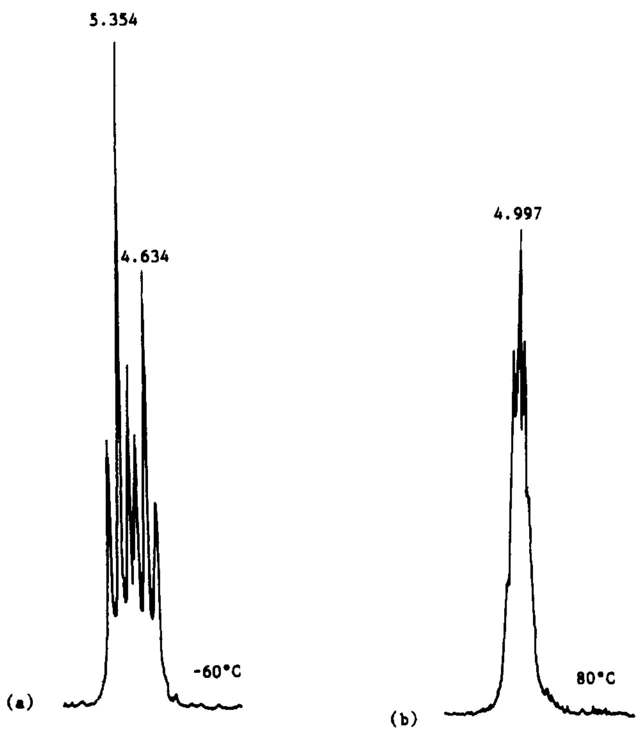

Figure 3. (a) Low-limiting and (b) high-limiting $^{31}P\{^1H\}$ NMR spectra of **3a**/**3b** (40.25 MHz).

It is interesting to note that for this series of compounds the chemical shifts due to axial carbonyls appear at higher field than those attributed to the equatorial carbonyls. This is opposite to what is found in similar molecules where silyl groups are not fluorinated.[15] It seems that the electronic effect of the fluorosilyl groups has considerable influence on the ^{13}C chemical shifts of the carbonyls.

The dynamic behaviors shown in the ^{19}F, ^{31}P, and ^{13}C NMR spectra indicate that **3a** and **3b** undergo rapid fluxion, which results in the isomerization between **3a** and **3b**. The kinetic parameters derived from these three kinds of spectra are in good agreement with each other (Table VI).

Discussion

Since P–F couplings are retained in the fast-exchange spectra (Figure 3b) and the ^{13}C labeling experiment shows no CO exchange under the experimental conditions used, any dissociative pathway that would lead to the observed ligand permutation is ruled out. Only the intramolecular pathways are considered.

For complexes of the type $F_2SiC(t\text{-}Bu){=}CHSiF_2Fe(CO)_3$-(phosphine), it is understood that any intramolecular rearrangement process that would put two silyl groups trans to each other is not likely. In principle, three configurations (a–c) could be involved in the dynamic system. However, since c has not been observed in the low-limiting spectrum, one assumes that only a and b are to be considered. In fact both electronic and steric arguments would not favor an axial phosphine ligand (c) in such complexes (fluorosilyl group is a stronger π ligand than CO). The known fact that axial carbonyl ligands tend to tilt considerably toward the silyl groups[18] would especially favor a bulky phosphine at an equatorial position.

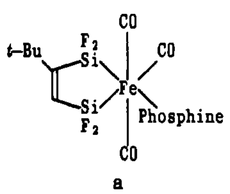

a

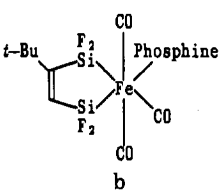

b

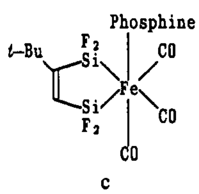

c

Complexes such as **3a** and **3b** belong to the point group C_s with two symmetry elements E and σ. When the conditions described above are applied, there are 3!2! = 12 possible permutations that convert a labeled complex into all possible labeled complexes with the configurations a and b as shown.[20]

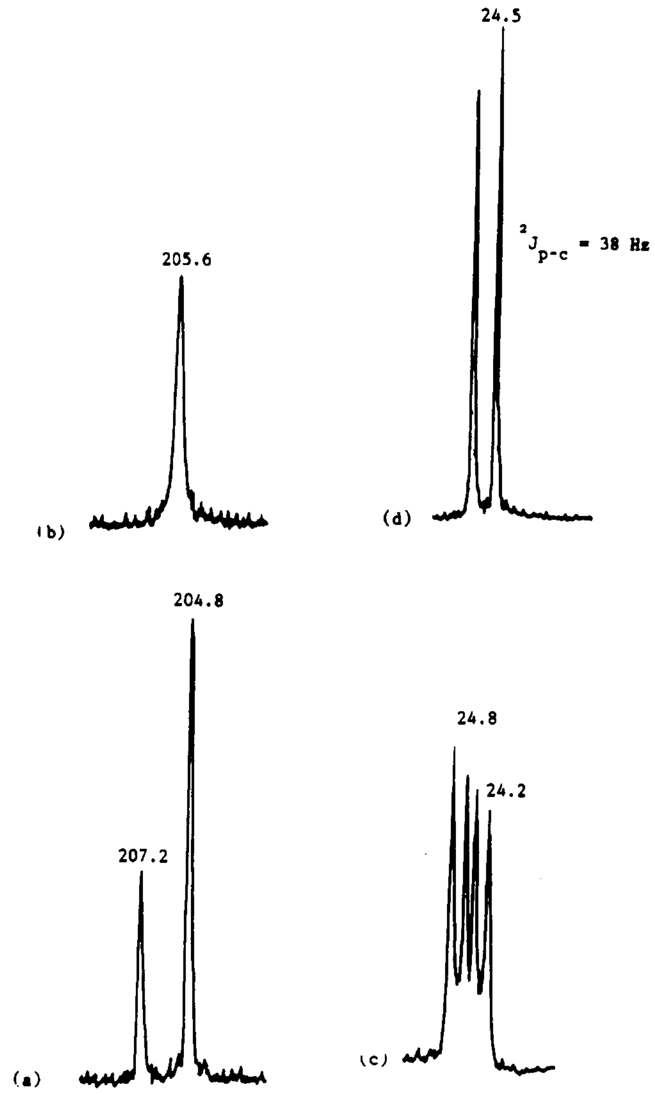

Figure 4. 100.1-MHz $^{13}C\{^1H\}$ spectra of the carbonyls of **3a**/**3b** at (1) −50 °C and (b) 100 °C (only the CO region is shown) and $^{13}C\{^1H\}$ spectra of PMe_3 of **3a**/**3b** at (c) −50 °C and (d) 100 °C.

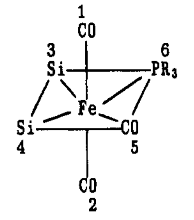

Three pathways of permutation are considered here; they are namely "tetrahedral jump", "2-fold twist", and "trigonal twist".

The exchange pathway of a tetrahedral jump is not very likely because the distortions from octahedra for these complexes are relatively small. Besides, if configurations involving trans silyl groups or axial phosphine are avoided, the basic permutation set can be simplified as follows:

$$\begin{array}{ccc} (1\ 2\ 3\ 4\ 5\ 6) & & (2\ 5) \\ (1\ 5\ 3\ 4\ 2\ 6) & = & \\ (5\ 2\ 3\ 4\ 1\ 6) & & (1\ 5) \end{array}$$

Although such permutations would allow the exchange of environments of the carbonyl groups, no averaged spectra of ^{19}F and ^{31}P are expected.

Table VI. ΔG^* and Coalescence Temperatures for Compounds **3**–**6**

compd	NMR nuclei	chem shift,[a] δ	T_c,[b] K	ΔG^*,[c] kcal/mol
3a/**3b**	^{13}C	187.5, 188.3	343	16.7
		151.1, 150.4	343	16.7
	^{19}F	90.15, 92.64	363	16.8
		100.73, 103.25	363	16.8
	^{31}P	5.35, 4.63	333	16.7
4a/**4b**	^{19}F	89.85, 91.28	323	15.2
		100.74, 102.24	323	15.2
	^{31}P	61.6, 62.18	295	14.9
5a/**5b**	^{19}F	90.4, 94.1	278	12.5
		101.3, 105.2	278	12.5
	^{31}P	−11.4, −12.45	255	12.5
6a/**6b**	^{19}F	85.57, 86.7	288	13.6
		96.0, 96.6	268	13.1

[a] Chemical shift in low-limiting spectra; chemical shifts of $=C(t\text{-Bu})$ and $=CHSiF_2$ are used. [b] Coalescence temperature. [c] Calculated by using coalescence temperature of pairs of NMR signals,[a] assuming equal populations of the two isomers (fairly good approximation).

The second possible pathway of intramolecular rearrangement is a 2-fold twist about the axis bisecting angles Si–Fe–Si and P–Fe–CO_{eq}. The basic permutation set is simple:

$$\begin{array}{c} (1\ 2\ 3\ 4\ 5\ 6) \\ \\ (1\ 2\ 3\ 4\ 6\ 5) \end{array} = (5\ 6)$$

Such process would lead to the averaging of the ^{19}F and ^{31}P spectra but not the ^{13}C spectrum of the carbonyl groups. In other words, exchange between the axial and equatorial CO groups cannot be achieved.

The third possible pathway to be considered is the trigonal-twist or Bailar mechanism. If the constraints described above are adopted, the basic permutation set can be written as follows:

$$\begin{array}{c} (1\ 2\ 3\ 4\ 5\ 6) \\ (1\ 5\ 3\ 4\ 6\ 2) \\ (5\ 2\ 3\ 4\ 6\ 1) \end{array} = \begin{array}{c} (2\ 5\ 6) \\ \\ (1\ 5\ 6) \end{array}$$

It is obvious that permutation of ligands according to this basic set would give the results observed experimentally, i.e., the merge of four different SiF_2 chemical environments into two, two different CO into one, and two different PR_3 into one.

This exchange pathway of partially restricted trigonal twist is performed about the pseudo-3-fold axes. For example, in Figure 5 a counterclockwise trigonal rotation about axis α would first shift ligands of A into structure B. Continued twist about axis α would inevitably result in the unfavored configuration where the phosphine occupies the axial position. Meanwhile, an equally facile counterclockwise trigonal twist about axis β can shift the ligands into structure C.

Thus, the combination of such partially restricted trigonal twists would lead to the isomerization that provides the facile pathways for all the ligand permutations observed experimentally.

It is noteworthy that the rate of such intramolecular polytopal rearrangement increases in the order $PMe_3 < PMePh_2 < PPh_3 \approx PEt_3$.

This order seems to suggest that, at least for the series of $\overline{F_2SiC(t\text{-Bu})=CHSiF_2Fe}(CO)_3(\text{phosphine})$, the distortion from a regular octahedron caused by the steric effect of the phosphine is mainly responsible for the rate of such a polytopal rearrangement process. The increase in rate of rearrangement with increasing steric bulk of the phosphines is opposite to the results reported for the series of bis-chelate compounds $MX_2(L\text{-}L)_2$.[7] It has been shown that increase in the bulk of ligand X would slow down the rearrangement rate of a trigonal-twist process because the increase in crowdedness in the trigonal-prismatic transition state is more pronounced than that in the octahedral ground state. However, in the present case of monochelate complexes, where the axial carbonyl ligands are known to tilt toward the silyl groups, the bulk of a phosphine ligand would enhance the distortion. It is interesting to note that in the trigonal-prismatic transition state of both "partially restricted trigonal twist" processes shown in Figure 5, the ligand eclipsed to the bulky phosphine is the carbonyl that tilts toward the silyl groups. Such a distortion is expected to relieve more effectively the crowdedness of the transition state. Thus, **5a**/**5b**, with a larger phosphine ligand PPh_3 and higher degree of distortion (CO_{ax}–Fe–CO_{ax} = 163.6 (11)° for **5a**), undergoes faster ligand permutation than **3a**/**3b**, which has a smaller ligand PMe_3 and less distortion about the CO_{ax}–Fe–CO_{ax} angle (168 (1)° for **3b**). As the distortion becomes more pronounced, other processes of permutation may become possible.[11,12]

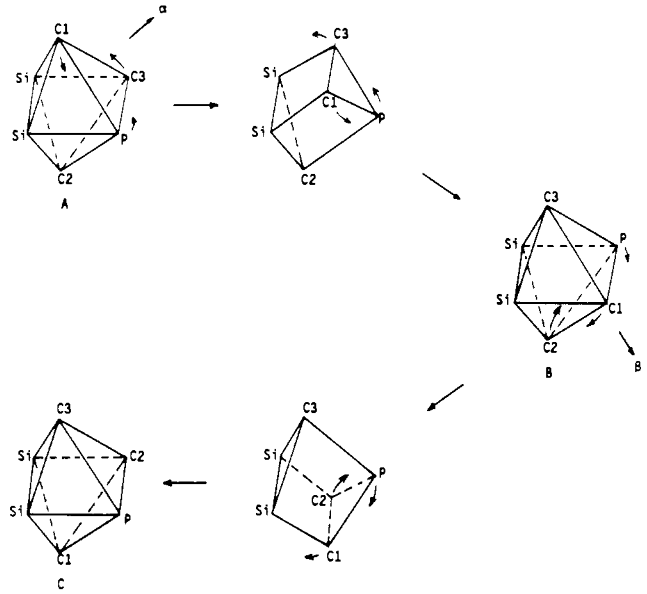

Figure 5. Schematic trigonal-twist mechanism for a distorted octahedron. Note that the carbonyls eclipsed to the phosphine in the two prismatic transition states (C2 and C3, respectively) are tilted toward the silyl groups.

Experimental Section

Vacuum distillations and manipulations were carried out by use of vacuum lines at 10^{-3} Torr; solvents were dried and distilled over calcium hydride. The phosphines (Strem) and $Fe(CO)_5$ (Merck) were used as received. The compounds **1** and **2** were prepared according to literature references published elsewhere.[21,22]

Spectra. All mass spectra were recorded on a JEOL JMS-100 mass spectrometer operating at 12 eV. The NMR spectra were obtained from a JEOL JMS FX-100 spectrometer operating at 99.55, 93.65, 40.25, and 25.0 MHz for ^1H, ^{19}F, ^{31}P, and ^{13}C NMR spectra, respectively, and a Bruker AM400 spectrometer operating at 400.1, 376.5, 161.5, and 100.1 MHz for ^1H, ^{19}F, ^{31}P, and ^{13}C NMR spectra, respectively. All values were measured in δ; ^{19}F NMR chemical shifts were measured in parts per million upfield from the internal standard CCl_3F. The IR spectra were obtained from a Bomen MB-100 spectrometer; *n*-hexane was used as the solvent for the sample.

Preparations of 3a/3b, 4a/4b, 5a/5b, and 6a/6b. A mixture of 383 mg (1.0 mmol) of compound **2** and an equal molar amount of phosphine (PMe_3 for compounds **3a**/**3b**, $PMePh_2$ for compounds **4a**/**4b**, PPh_2 for compounds **5a**/**5b**, and PEt_3 for compounds **6a**/**6b**) in 10 mL of dried *n*-hexane was degassed and then frozen at −196 °C, and the reaction tube was sealed under vacuum. The reaction tube was then heated at 160 °C for 72 h. Single crystals of those compounds were obtained by recrystallization in dried, degassed *n*-pentane solution at −5 °C. All handlings must be carried out under inert atmosphere. The yields based on the quantity of **2** used are 75% (**3a**/**3b**), 82% (**4a**/**4b**), 85% (**5a**/**5b**), and 83% (**6a**/**6b**). The NMR spectra were obtained at low temperature.

Analytical data for compounds **3a** and **3b** are as follows. Anal. Calcd: C, 33.49; H, 4.42; F, 17.76. Found: C, 33.45; H, 4.48; F, 17.70. Mass spectrum: *m/e* 430 (M^+, $C_{12}H_{19}Si_2F_4O_3PFe^+$), 402 ($C_{11}H_{19}Si_2F_4O_2PFe^+$), 374 ($C_{10}H_{19}Si_2F_4OPFe^+$), 346 ($C_9H_{19}Si_2F_4PFe^+$), 216 ($C_6H_9O_3PFe^+$), 188 ($C_5H_9O_2PFe^+$), 160 ($C_4H_9OPFe^+$), 132 ($C_3H_9PFe^+$). ^1H NMR: δ 1.1 (s), 9 H, *t*-Bu; δ 1.2 (d), 9 H, $P(CH_3)_3$; δ 7.05 (m), 1 H, $=CHSiF_2$. ^{13}C NMR: δ 30.13 s (q), $C(CH_3)_3$; δ 38.6

s (s), $\mathrm{\mathit{C}(CH_3)_3}$; δ 24.2 and 24.8 s (q), $\mathrm{P(\mathit{C}H_3)_3}$ of **3a** or **3b**; δ 151.1 and 150.4 m (dm), $\mathrm{{=}\mathit{C}HSiF_2}$ of **3a** or **3b**; δ 187.5 and 188.3 m (m), $\mathrm{{=}\mathit{C}(\mathit{t}\text{-}Bu)SiF_2}$ of **3a** or **3b**; δ 204.8 (br), CO of **3a** and **3b** at axial position; δ 207.2 (br), CO of **3a** and **3b** at equatorial position. $^{19}\mathrm{F}\{^1\mathrm{H}\}$ NMR for compound **3a**: δ 100.73 (d, $^3J_{\mathrm{F-P}} = 10.5$ Hz), $\mathrm{{=}C(\mathit{t}\text{-}Bu)Si\mathit{F}_2}$; δ 92.64 (s), $\mathrm{{=}CHSi\mathit{F}_2}$. $^{19}\mathrm{F}$ NMR for compound **3b**: δ 103.25 (s), $\mathrm{{=}C(\mathit{t}\text{-}Bu)Si\mathit{F}_2}$; δ 90.15 (d, $^3J_{\mathrm{F-P}} = 10.8$ Hz), $\mathrm{{=}CHSi\mathit{F}_2}$. $^{31}\mathrm{P}\{^1\mathrm{H}\}$ NMR: δ 5.35 (t) and 4.63 (t) for compounds **3a** and **3b**. IR (ν_{CO}): 2117 (s), 2056 (s), 2036 (s), 1979 (s) cm^{-1}.

Analytical data for compounds **4a** and **4b** are as follows. Anal. Calcd: C, 47.65; H, 4.15; F, 13.72. Found: C, 47.60; H, 4.18; F, 13.79. Mass spectrum: *m/e* 554 ($\mathrm{M^+}$, $\mathrm{C_{22}H_{23}Si_2F_4O_3PFe^+}$), 526 ($\mathrm{C_{21}H_{23}Si_2F_4O_2PFe^+}$), 498 ($\mathrm{C_{20}H_{23}Si_2F_4OPFe^+}$), 470 ($\mathrm{C_{19}H_{23}Si_2F_4PFe^+}$), 340 ($\mathrm{C_{16}H_{13}O_3PFe^+}$), 312 ($\mathrm{C_{15}H_{13}O_2PFe^+}$), 284 ($\mathrm{C_{14}H_{13}OPFe^+}$), 256 ($\mathrm{C_{13}H_{13}PFe^+}$). ^{1}H NMR: δ 1.1 (s), 9 H, *t*-Bu; δ 1.3 (d), 3 H, $\mathrm{P(C\mathit{H}_3)}$; δ 7.2–7.5 (c), 11 H, $\mathrm{{=}C\mathit{H}SiF_2}$ and protons for phenyl ring. ^{13}C NMR: δ 30.1 s (q), $\mathrm{C(\mathit{C}H_3)_3}$; δ 16.4 d (m), $\mathrm{P(\mathit{C}H_3)}$; δ 38.7 s (s), $\mathrm{\mathit{C}(CH_3)_3}$; δ 132.7 d (d), $\mathrm{P{-}\mathit{C}(CH)_2}$; δ 128.6 s (d), $\mathrm{P{-}C(\mathit{C}H)_2}$; δ 131.1 s (d), $\mathrm{\mathit{C}H(CH)_2}$; δ 132.6 s (d), $\mathrm{CH(\mathit{C}H)_2}$; δ 151.1 m (dm), $\mathrm{{=}\mathit{C}HSiF_2}$; δ 187.9 m (m), $\mathrm{{=}\mathit{C}(\mathit{t}\text{-}Bu)SiF_2}$; δ 205.4, CO at axial position; δ 208.5, CO at equatoral position. $^{19}\mathrm{F}\{^1\mathrm{H}\}$ for **4a**: δ 91.28 (s, $\mathrm{{=}CHSi\mathit{F}_2}$); δ 100.74 (d, $^3J_{\mathrm{F-P}} = 10.4$ Hz), $\mathrm{{=}C(\mathit{t}\text{-}Bu)Si\mathit{F}_2}$. $^{19}\mathrm{F}\{^1\mathrm{H}\}$ NMR for **4b**: δ 89.85 (d, $^3J_{\mathrm{F-P}} = 10.6$ Hz), $\mathrm{{=}CHSiF_2}$; δ 102.24 (s), $\mathrm{{=}C(\mathit{t}\text{-}Bu)Si\mathit{F}_2}$. $^{31}\mathrm{P}\{^1\mathrm{H}\}$ NMR: δ 61.6 (t) and 62.18 (t) for compounds **4a** and **4b**. IR (ν_{CO}): 2114 (m), 2040 (br), 1983 (s) cm^{-1}.

Analytical data for compounds **5a** and **5b** are as follows. Anal. Calcd: C, 52.60; H, 4.06; F, 12.34. Found: C, 52.66; H, 4.10; F, 12.38. Mass spectrum: *m/e* 616 ($\mathrm{M^+}$, $\mathrm{C_{27}H_{25}Si_2F_4O_3PFe^+}$), 588 ($\mathrm{C_{26}H_{25}Si_2F_4O_2PFe^+}$), 560 ($\mathrm{C_{25}H_{25}Si_2F_4OPFe^+}$), 532 ($\mathrm{C_{24}H_{25}Si_2F_4PFe^+}$), 402 ($\mathrm{C_{21}H_{15}O_3PFe^+}$), 374 ($\mathrm{C_{20}H_{15}O_2PFe^+}$), 346 ($\mathrm{C_{19}H_{15}OPFe^+}$), 318 ($\mathrm{C_{18}H_{15}PFe^+}$). ^{1}H NMR: δ 1.1 (s) and 1.0 (s), 18 H, *t*-Bu; δ 7.0–7.6 (br), 32 H, $\mathrm{{=}C\mathit{H}SiF_2}$ and proton of phenyl ring. ^{13}C NMR: δ 29.2 s (q), 29.3 s (q), $\mathrm{C(\mathit{C}H_3)_3}$; δ 38.4 s (s), 38.6 s (s), $\mathrm{\mathit{C}(CH_3)_3}$; δ 133.2 d (d), 133.26 d (d), $\mathrm{P{-}\mathit{C}(CH)_2}$; δ 130.7 s (d), $\mathrm{\mathit{C}H(CH)_2}$; δ 128.7 s (d) and 132.7 s (d), $\mathrm{P{-}C(\mathit{C}H)_2}$ and $\mathrm{CH(\mathit{C}H)_2}$; δ 147.7 m (dm) and 151.6 m (dm), $\mathrm{{=}\mathit{C}HSiF_2}$; δ 188.1 m (m) and 185.3 m (m), $\mathrm{{=}\mathit{C}(\mathit{t}\text{-}Bu)SiF_2}$; δ 205, CO at axial position; δ 207.3, CO at equatorial position. $^{19}\mathrm{F}\{^1\mathrm{H}\}$ NMR for **5a**: δ 101.3 (d, $^3J_{\mathrm{F-P}} = 10.8$ Hz), $\mathrm{{=}C(\mathit{t}\text{-}Bu)Si\mathit{F}_2}$; δ 94.1 (s), $\mathrm{{=}CHSi\mathit{F}_2}$. $^{19}\mathrm{F}\{^1\mathrm{H}\}$ NMR for **5b**: δ 105.2 (s), $\mathrm{{=}C(\mathit{t}\text{-}Bu)Si\mathit{F}_2}$; δ 90.4 (d, $^3J_{\mathrm{F-P}} = 10.8$ Hz), $\mathrm{{=}CHSi\mathit{F}_2}$. $^{31}\mathrm{P}\{^1\mathrm{H}\}$ NMR: δ −11.4 (t) and −12.45 (t) for compounds **5a** and **5b**. IR (ν_{CO}): 2113 (m), 2053 (br), 1983 (s) cm^{-1}.

Analytical data for compounds **6a** and **6b** are as follows. Anal. Calcd: C, 38.14; H, 5.30; F, 16.10. Found: C, 38.21; H, 5.34; F, 16.05. Mass spectrum: *m/e* 472 ($\mathrm{M^+}$, $\mathrm{C_{15}H_{25}O_3Si_2F_4PFe^+}$), 444 ($\mathrm{C_{14}H_{25}O_2Si_2F_4PFe^+}$), 416 ($\mathrm{C_{13}H_{25}OSi_2F_4PFe^+}$), 388 ($\mathrm{C_{12}H_{25}Si_2F_4PFe^+}$), 258 ($\mathrm{C_9H_{15}O_3PFe^+}$), 202 ($\mathrm{C_7H_{15}OPFe^+}$), 174 ($\mathrm{C_6H_{15}PFe^+}$). ^{1}H NMR: δ 1.1 (s), 9 H, *t*-Bu; δ 7.05 (m), 1 H, $\mathrm{{=}C\mathit{H}Si_2F_4}$; ^{13}C NMR: δ 29.5 s (q), $\mathrm{C(\mathit{C}H_3)_3}$; δ 38.5 s (s), $\mathrm{\mathit{C}(CH_3)_3}$; δ 20.5 d (dt), $\mathrm{P(\mathit{C}H_2CH_3)_3}$; δ 8.5 d (dq), $\mathrm{P(CH_2\mathit{C}H_3)_3}$; δ 150.5 m (dm), $\mathrm{{=}\mathit{C}HSiF_2}$; δ 187.5 m (m), $\mathrm{{=}\mathit{C}(\mathit{t}\text{-}Bu)SiF_2}$; δ 205.2, CO at axial position; δ 207.4, CO at equatorial position. $^{19}\mathrm{F}\{^1\mathrm{H}\}$ NMR for **6a**: δ 86.7 s, $\mathrm{{=}CHSi\mathit{F}_2}$; δ 96.0 (d, $^3J_{\mathrm{F-P}} = 11$ Hz), $\mathrm{{=}C(\mathit{t}\text{-}Bu)Si\mathit{F}_2}$. $^{19}\mathrm{F}\{^1\mathrm{H}\}$ NMR for compound **6b**: δ 85.57 (d, $^3J_{\mathrm{F-P}} = 10.7$ Hz), $\mathrm{{=}CHSi\mathit{F}_2}$; δ 96.6 s, $\mathrm{{=}C(\mathit{t}\text{-}Bu)Si\mathit{F}_2}$. IR ($\nu_{\mathrm{CO}}$): 2047 (s), 1982 (s), 1929 (s), 1865 (s) cm^{-1}.

CO Exchange. Tests of CO exchange were carried out in a 50-mL bulb connected to the vacuum line. Samples of 10 mL of an *n*-hexane solution containing approximately 0.3 mmol of $\mathrm{F_2SiC(\mathit{t}\text{-}Bu){=}CHSiF_2Fe(CO)_3(phosphine)}$ were degased, and a pressure of 1 atm of ^{13}CO (99% isotope purity, CIL) was admitted to the bulb at −78 °C. The solution was stirred at 50 °C for 24 h (the estimated pressure was about 1.6 atm). After removal of ^{13}CO and solvent, the samples were examined by mass spectrometry. No enrichment was observed for the whole series of $\mathrm{F_2SiC(\mathit{t}\text{-}Bu){=}CHSiF_2Fe(CO)_3(phosphine)}$ compounds.

Determination of the Crystal and Molecular Structures of 3b and 5a. The intensities of both **3b** and **5a** were measured on a CAD4 diffractometer, using monochromated Mo Kα radiation ($\lambda = 0.7107$ Å), with the $\theta/2\theta$ scan technique. Three reflections were monitored every 1 h throughout the measurements; linear decays of 6% and 12% were observed for compounds **3b** and **5a**, respectively. The intensities were scaled accordingly. The absorption correction was based on the experimental Ψ rotation. Other experimental details are given in Table I. The structures were solved by the heavy-atom method. Atomic parameters were obtained from the full-matrix least-squares refinements. The results are given in Tables II and III. The weights were based on counting statistics. Selected bond distances and angles are presented in Tables IV and V. The structure analyses were carried out on a Microvax computer using NRCVAX programs.[23] The atomic scattering amplitudes were taken from ref 25.

Acknowledgment. We thank the National Science Council for financial support of this work. C.Y.L. thanks the NSC for a postdoctoral fellowship.

Supplementary Material Available: Tables of complete atomic coordinates and isotropic thermal parameters, bond distances and angles, and anisotropic thermal parameters for compounds **3b** and **5a** (11 pages); listings of observed and calculated structure factors for **3b** and **5a** (22 pages). Ordering information is given on any current masthead page.

---

(25) *International Tables for X-ray Crystallography*; Kynoch: Birmingham, U.K., 1982; Vol. IV.